Applied Surface Science 257 (2011) 5443–5446

Contents lists available at ScienceDirect

Applied Surface Science

journal homepage: www.elsevier.com/locate/apsusc

Modeling of femtosecond ablation of aluminum film with single laser pulses

A.V. Mazhukin*, V.I. Mazhukin, M.M. Demin

Institute of Mathematical Modeling of RAS, 4a Miusskaya sqr., 125047 Moscow, Russia

ARTICLE INFO

Article history:
Available online 15 December 2010

Keywords:
Modeling
Femtosecond
Ablation
Non-equilibrium
Phase transition

ABSTRACT

Detailed investigation of pulsed laser ablation dynamics is performed for aluminum target under action of 100 fs pulses with peak intensity 3.95×10^{12} W/cm^2 and wavelength 0.8 μm.Non-equilibrium two-temperature model with hydrodynamic Stephan problem was used for modeling. Explicit tracking of moving interphase boundaries permits exact determination of their velocity and amount of removed and evaporated material. Detailed ablation process is analyzed using the study of temperature, pressure and density evolution in the target. High phase front velocities (melting up to 5 km/s and evaporation up to 350 m/s) are caused by strong overheating of solid and liquid phases.

1. Introduction

The investigation of the fundamental problem of femtosecond laser ablation is far from its completion. Despite of the impressive achievements of the theoretical works on the material removal mechanisms including evaporation, phase explosion, spallation, etc. during previous 10 years [1–3], several problems remain unclear. High non-equilibrium state of the processes of the laser heating with the ultrashort pulses and associated with them fast phase change dynamics complicate the determination of the dominating ablation mechanisms and their interchange as the pulse duration and intensity changes. In particular, all the transport properties in the used models are highly non-equilibrium and are not known in the wide frequency and temperature range. These problems continue to stimulate further investigation of the femtosecond ablation.

The objective of this work is the detailed investigation of the dynamics of the femtosecond laser ablation using the numerical solution of the theoretical model describing ultrashort high-power laser action on metals in the approximation of the hydrodynamic type of two-temperature model with explicit tracking of interphase fronts.

2. Theoretical model

The laser radiation propagates from the right to the left and hits the metal target where it is partially absorbed and partially reflected. Fig. 1 shows the spatial phase distribution, the moving boundaries $\Gamma_{sl}(t)$, $\Gamma_{lv}(t)$, $\Gamma_{vg}(t)$ and the shock wave in solid $\Gamma_{sh,s}(t)$.

The statement of the problem includes the following assumptions.

a) The mechanisms of homogenous (volume) melting and evaporation are excluded from consideration.
b) It is supposed that the melting front appears at the irradiated surface when the temperature reaches the equilibrium melting temperature T_{m0} and the overheated metastable states behave in a stable way during the time of observation.

Mathematical description and modeling of femtosecond laser ablation of hard aluminum target is performed within the framework of two-temperature and spatially one-dimensional multi-front Stephan problem for two phases: solid and liquid.

$$\left(\begin{array}{l} \dfrac{\partial \rho}{\partial t} + \dfrac{\partial (\rho u)}{\partial x} = 0 \\ \dfrac{\partial (\rho u)}{\partial t} + \dfrac{\partial (\rho u^2)}{\partial x} + \dfrac{\partial P}{\partial x} = 0 \\ \dfrac{\partial (\rho_e \varepsilon_e)}{\partial t} + \dfrac{\partial (\rho_e u \varepsilon_e)}{\partial x} = -\left(P_e \dfrac{\partial u}{\partial x} + \dfrac{\partial W_e}{\partial x} + g(T_e)(T_e - T_{ph}) + \dfrac{\partial G}{\partial x} \right) \\ \dfrac{\partial (\rho \varepsilon_{ph})}{\partial t} = -\left(P_{ph} \dfrac{\partial u}{\partial x} + \dfrac{\partial W_{ph}}{\partial x} - g(T_e)(T_e - T_{ph}) \right) \\ \dfrac{\partial G}{\partial x} + \alpha(T_e) G = 0 \\ P = P(\rho, T), \quad \varepsilon_e = C_{ve}(T_e) T_e, \quad \varepsilon_{ph} = C_{vph}(T_{ph}) T_{ph} \end{array} \right)_{k=s,l},$$

$$t > 0, 0 < x < \Gamma_{sl} \cup \Gamma_{sl} < x < \Gamma_{lv}$$

where $W_e = -\lambda(T_e, T_{ph}) \partial T_e / \partial x$, $W_{ph} = -\lambda(T_{ph}) \partial T_{ph} / \partial x$, $P(\rho, T) = P(\rho_e, T_e) + P(\rho_{ph}, T_{ph})$, here ρ, u, ε, T and P are the density, gas-dynamic velocity, internal energy, temperature and pressure, $\alpha(T_e)$, $R(T_e)$ and G are the coefficient of volume absorption, surface reflectivity and laser radiation energy density, C_θ and λ are heat

* Corresponding author.
E-mail address: vim@modhef.ru (A.V. Mazhukin).

0169-4332/$ – see front matter.
doi:10.1016/j.apsusc.2010.11.154

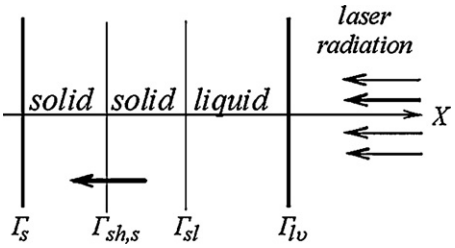

Fig. 1. Spatial phase configuration.

capacity and heat conductivity, $g(T_e)$ is the electron–phonon coupling factor. The indexes $k = s, l, \upsilon$ represent the solid, liquid and vapor phases, e, ph represent the electron and phonon gas.

The following boundary conditions were used on the interphase boundaries:

$$x = \Gamma_{sl}(t): \left(\lambda_e \frac{\partial T_e}{\partial x}\right)_s = \left(\lambda_e \frac{\partial T_e}{\partial x}\right)_l, \quad (T_e)_s = (T_e)_l,$$

$$\left(\lambda_{ph} \frac{\partial T_{ph}}{\partial x}\right)_s - \left(\lambda_{ph} \frac{\partial T_{ph}}{\partial x}\right)_\ell = \rho_s L_m^{ne} \upsilon_{sl}, \quad 4p_s + \rho_s \upsilon^2 = p_l + \rho_l (u_l - u_s - \upsilon_{sl})^2,$$

$$\rho_s \upsilon_{sl} = \rho_l (u_l - u_s - \upsilon_{sl}), \quad L_m^{ne} = L_m + \Delta C_{ps\ell}\, \Delta T_{s\ell} + \frac{\rho_s + \rho_\ell}{\rho_s - \rho_\ell} \frac{(u_s - u_\ell)^2}{2}$$

$$\Delta C_{ps\ell} = (C_{p\ell} - C_{ps}), \quad \Delta T_{s\ell} = (T_m(p_s) - T_m),\ T_m(p_s) = (T_{m,0} + \theta \cdot p_s),$$

$$T_{sl} = T_{ph,s} = T_{ph,l} = T_m(p_s),$$

where θ is a constant.

Note that the usage of the condition of the temperature equality at the interface is equivalent to the restriction of overheating of the solid surface:

$$x = \Gamma_{k\upsilon}(t), k = s, l, \quad -\lambda_e \frac{\partial T_e}{\partial x} = \sigma T_e^4, \quad \left(-\lambda_{ph} \frac{\partial T_{ph}}{\partial x}\right)_k = \rho_k L_\upsilon^{ne} \vartheta_{k\upsilon},$$

$$L_\upsilon^{ne} = L_\upsilon^e(T_\ell) + C_{p\upsilon}(T_b - T_{sur}) + \frac{\rho_\ell + \rho_\upsilon}{\rho_\ell - \rho_\upsilon} \frac{(u_\ell - u_\upsilon)^2}{2}, \quad \rho_k \upsilon_{k\upsilon} = \rho_\upsilon (u_k - u_\upsilon + \upsilon_{k\upsilon}),$$

$$P_k + \rho_k \upsilon_{k\upsilon} = p_\upsilon + \rho_\upsilon (u_k - u_\upsilon + \upsilon_{k\upsilon}), \quad T_\upsilon = \alpha_T(M) T_{ph,k}, \quad \rho_\upsilon = \alpha_\rho(M) \rho_{sat},$$

$$\rho_{sat} = \frac{p_{sat}(T_{ph,k})}{R T_{phk}}, \quad p_{sat}(T_{ph,k}) = p_b \exp\left(\frac{1}{T_b} - \frac{1}{T_{ph,k}}\right) \frac{L_\upsilon^{ne}}{R}, \quad k = s, 1$$

$$G(t) = (1 - R(T_e)) \cdot G_0 \exp\left(-\left(\frac{t}{\tau_L}\right)^2\right),$$

where υ_{ku} and $\upsilon_{s\ell}$ are the evaporation and melting velocity, L_υ^{ne} and L_m^{ne} are the non-equilibrium specific heat of evaporation and melting, $\alpha_T(M)$ and $\alpha_\rho(M)$ are the Crout coefficients [4], pb, T_b and T_m are the equilibrium evaporation pressure, the boiling and melting temperature, T_υ and ρ_υ are the vapor temperature and density, ρ_{sat} and p_{sat} are the density and pressure of saturated vapor, σ is the Stephan–Boltzmann constant.

In order to determine the transport and optical characteristics $\lambda_e(T_e, T_{ph})$, $\lambda_{ph}(T_{ph})$, $g(T_e)$, $\alpha(T_e)$, $R(T_e)$ we used the approach [5] that allow us to obtain the following dependencies for arbitrary temperature range:

$$\left(\lambda_e(T_e, T_{ph})\right)_k = \left(C_{ve}(T_e) \chi_e(T_e, T_{ph})\right)_k = \left(\frac{1}{3} C_{ve}(T_e) \ell_e(T_e, T_{ph}) \left\langle \upsilon_e(T_e) \right\rangle\right)_k,$$

where $\chi_e(T_e, T_{ph})$ is the averaged temperature conductivity of electron Fermi-gas, $\left\langle \upsilon_e(T_e) \right\rangle = (3/2)^{1/2}(9\pi/4)^{1/3}(z^{1/3}/r)(\hbar/m_e)(\xi^2 + 0.16)^{1/4}$ is the mean electron velocity, $(\chi_e(T_e, T_{ph}))_k = ((\chi_{ee}(T_e)\chi_{eph}(T_e, T_{ph}))/(\chi_{ee} + \chi_{eph}))_k = (((\ell_{ee}(T_e)\ell_{eph}(T_{ph}))/(3(\ell_{ee}(T_e) + \ell_{eph}(T_{ph}))))_k \left\langle \upsilon_e(T_e) \right\rangle$, χ_{ee}, χ_{eph}, ℓ_{ee}, ℓ_{eph} are the temperature conductivity and free path for electron–electron and electron–phonon interaction [6]:

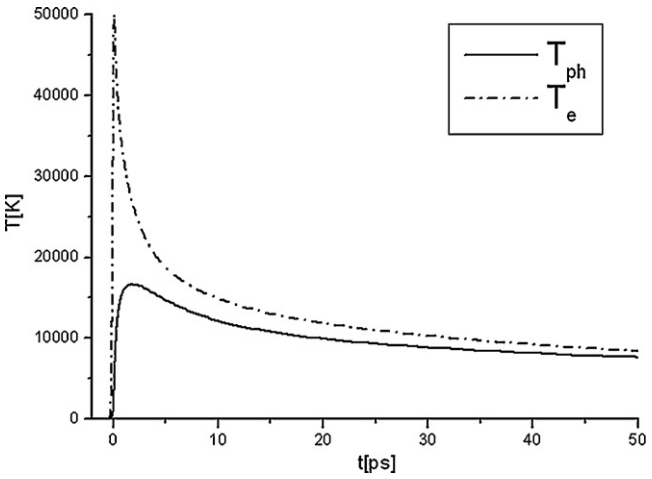

Fig. 2. Time dependencies of surface phonon and electron temperature.

$$l_{ee}(T_e) = \frac{1}{N_e \sigma_{ee}} = \frac{2}{\pi^2}\left(\frac{4}{9\pi}\right)^{1/3} \frac{1}{r^2} \frac{1}{z^{1/3} N_a} \cdot \frac{t^2}{\xi^2} \left[\ln(1+t) - \frac{t}{1+t}\right]^{-1},$$

$$(\ell_{eph}(T_{ph}))_k = \left(\frac{E_k \cdot r}{z N_a k_B T_{ph}}\right)_k$$

$r = ((3/4\pi)(1/N_a))^{1/3} = 0.6204 N_a^{-1/3}$ is the interatomic distance, $r_B = \hbar^2/m_e e^2$ is the Bohr radius, $\hbar$ is the Planck constant, k_B is the Boltzmann constant, m_e, e are the mass and charge of electron, z is the valence, N_a and N_e are the density of atoms and electrons, M_0 and A are the atomic mass unit and atomic weight.

Temperature dependency of electron–phonon coupling factor $g(T_e)$ is determined by the following expression [5]:

$$g(T_e) = \left\langle \Delta\varepsilon \right\rangle \frac{k_B N_e}{\varepsilon_F} = \left(\frac{3}{2}\right)^{1/2} \left(\frac{8}{9\pi}\right)^{1/3} \frac{8}{3} \cdot \frac{\hbar k_B}{r_B^2 M_0} \frac{z^2}{A} N_a \left[1 - \left(\frac{1}{2^4 z}\right)\right] \Phi_{eph}(\xi),$$

where $\left\langle \Delta\varepsilon \right\rangle$ is the average energy that is transferred during one collision of electron with phonon:

$$\Phi_{eph}(\xi) = \frac{\xi \cdot [\ln(t_1 + 1) - (t_1/(t_1 + 1))]}{(\xi^2 + 0.16)^{1/4}(\xi^2 + (4/9))^{1/2}}, \quad t_1 = \left(\frac{9\pi}{4}\right)^{4/3} \frac{z^{1/3}}{2} \frac{r_B}{r} \cdot \left[(\xi^2 + 0.16) \cdot \left(\xi^2 + \frac{4}{9}\right)\right]^{1/2}.$$

The temperature dependencies of the optical characteristics $\alpha(T_e)$ and $R(T_e)$ were taken from Ref. [7]. The equation of state $P = P(\rho, T)$ was taken from Refs. [8,9].

3. Results and discussion

Here we analyze the processes taking place in the aluminum target under the action of the laser pulse with duration $\tau_L = 100$ fs and intencity $G_0 = 3.95 \times 10^{12}$ W/cm^2 corresponding to the fluence of 0.7 J/cm^2 and wavelength $\lambda_L = 0.8$ μm.

All peculiarities of the femtosecond laser ablation are determined by a single factor: very high heat deposition rate. Figs. 2–4 show time dependencies of the surface temperature $T_e(t)$, $T_{ph}(t)$, electron–phonon coupling factor $g(t)$ and heat conductivity $\lambda_e(t)$. The time dependence $T_e(t)$ resembles the shape of the pulse with the maximum of $T_{emax}(t) \approx 5 \times 10^4$ K right after the peak intensity. The rapid rise of the electron temperature causes the rise of $g(t)$ and $\lambda_e(t)$. The electron–phonon coupling factor $g(t)$ increases by two orders of magnitude, from 10^{10} W/(cm^3 K) at $T_e = 300$ K, to 2×10^{12} W/(cm^3 K) at $T_{emax}(t)$. The maximum value of the lattice

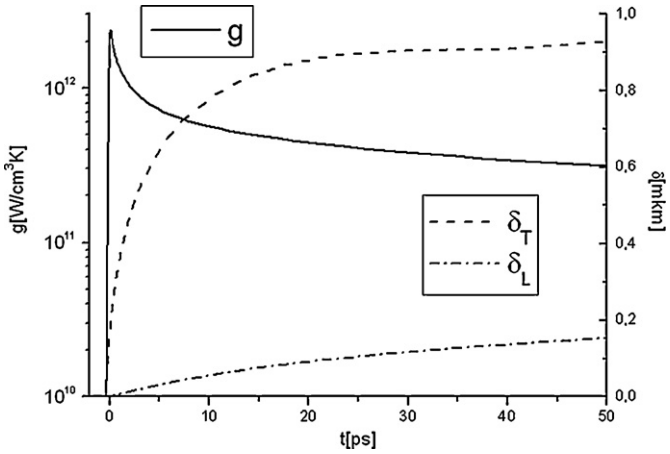

Fig. 3. Time dependence of energy exchange coefficient, heat zone and liquid size.

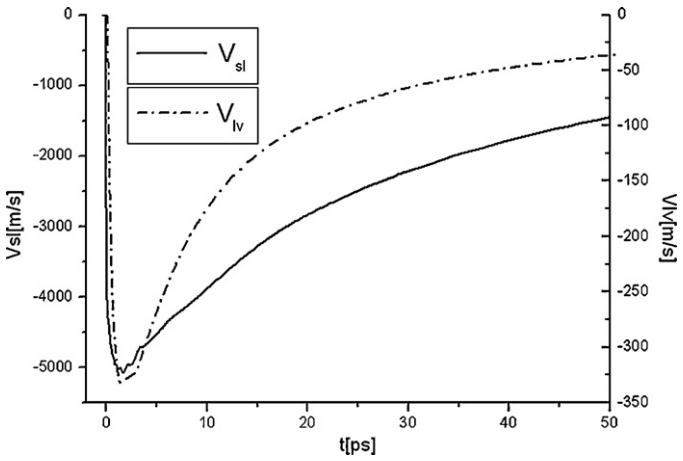

Fig. 5. Time dependence of melting and evaporation velocity.

temperature is reached at the end of the pulse $T_{ph,\max} \approx 1.6 \times 10^4$ K. This value is several times larger than the critical temperature T_{cr}. Theoretical possibility of such mode of femtosecond heating was shown in Ref. [2] using molecular dynamics. It is not possible to model further decomposition of the overheated state within the framework of the used continuum model. So we can only suggest that the mechanism of decomposition of the overheated state would be phase separation [2]. Complete temperature equilibration $T_e \approx T_{ph}$ for the described mode occurs at $t \approx 100$ ps.

The high heating rate determines the high rate of the phase transformations. Fig. 5 shows the time dependence of the velocity of melting $\upsilon_{sl}(t)$ and evaporation $\upsilon_{\ell\upsilon}(t)$ fronts. The melting process starts at the front slope of the laser pulse and reaches the maximum of $\upsilon_{sl\max}(t) \approx 5$ km/s. The surface evaporation starts with a certain delay. The maximum evaporation velocity is by one order lower than the one of the melting velocity due to the large value of specific energy of evaporation $L_\upsilon^{ne}(L_\upsilon^{ne} \gg L_m^{ne})$: $\upsilon_{\ell\upsilon\max}(t) \approx 350$ m/s. The high velocities of the propagation of the phase fronts are associated with the high material flow over the interphase boundaries. Together with the volume type of energy transfer from the electron gas to the lattice, this results in formation of highly overheated metastable states and appearance of subsurface maximums of temperature in solid and liquid, Fig. 6. Since the maximum velocity of the melting front appears to be comparable to the sound velocity $\upsilon_{sl\max}(t) \approx \upsilon_{\text{sound}}$, a shock wave is formed in the solid phase moving in front of the melting boundary, Fig. 6. Dotted lines mark the location of the phase fronts and the shock wave. Arrows show the location and the value of the temperature maximums. Since the overheating of the solid phase surface is restricted by the temperature equality condition $T_{sl} = T_{ph,s} = T_{ph,l} = T_m(p_s)$ the subsurface temperature maximum reaches the value of $\Delta T_{sl} = (T_{ph,s} - T_{ph,\max}) \approx 15000K$. Boundary conditions at the irradiated liquid surface do not contain the condition of the temperature equality $(T_{ph,\ell} = T_b)$ so it can be overheated. Therefore the subsurface temperature maximum turns out to be significantly less: $\Delta T_{l\upsilon} = (T_{ph,\ell} - T_{ph,\max}) \approx 5000$ K. Note that these temperature values are obtained under the assumption of the stability of the overheated states and the absence of the homogenous phase transitions (which description cannot be fulfilled within the framework of the continuum model).

The formation of the highly non-equilibrium region $T_e \gg T_{ph}$ is accompanied by the significant rise of the heat conductivity $\lambda_e(T_e, T_{ph})$ by 30 times, Fig. 4, which results in the propagation of the electron gas energy within very high volume, $\delta_T \approx 0.9$ μm, Fig. 3. The thickness of liquid phase at the time of $t = 50$ ps reaches ~180 nm, Fig. 7.

The usage of double pulses results in significant change and complication of the involved processes. Fig. 7 shows time dependence of the temperature for two pulses shifted by 10 ps.

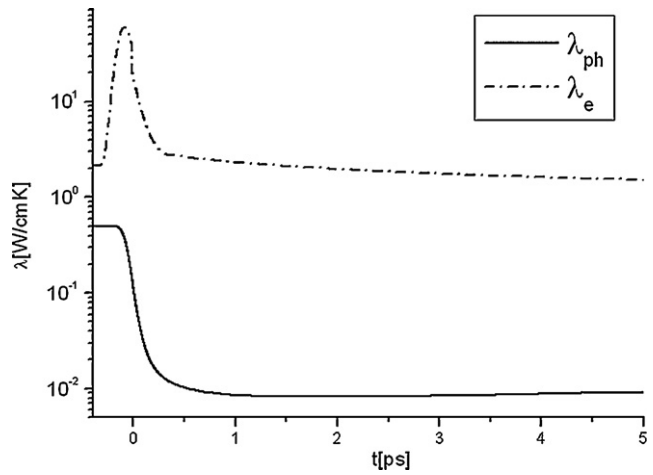

Fig. 4. Time dependence of phonon and electron heat conductivity.

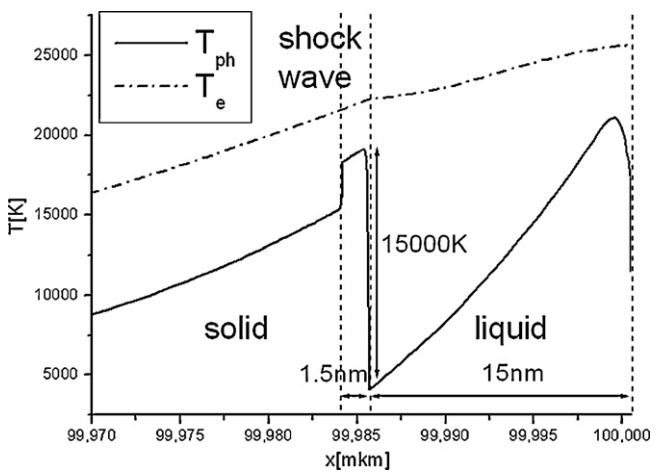

Fig. 6. Spatial profiles of phonon and electron temperature at $t = +2$ ps.

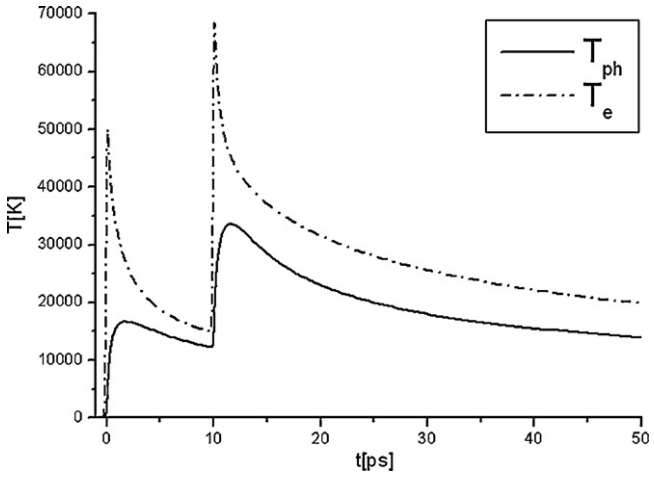

Fig. 7. Time dependence of phonon and electron temperature for 2 pulses.

4. Conclusion

The regime of laser femtosecond ablation of an aluminum target that is typical for laser treatment of materials is considered. Simulation results show qualitative influence of metastable overheated states on the basic processes. The delayed exchange of energy between electron and phonon subsystems with increased deposition of the energy of electronic gas leads to the volume type of heating of the lattice. Rapid phase transformations are accompanied by the occurrence of the strongly overheated (5,000–15,000 K) metastable states and shock waves in solid. At the same time, the definition of the mechanism of the decay of the overheated metastable states requires the addition of the discrete models of the type of molecular dynamics to the used continuum model.

Acknowledgments

This work was supported by the Russian Foundation for Basic Research, project nos. 10-07-00246a and 09-07-0225a.

References

[1] Z. Lin, L.V. Zhigilei, V. Celli, Electron–phonon coupling and electron heat capacity of metals under conditions of strong electron–phonon nonequilibrium, Phys. Rev. B 77 (2008) 075133-1–175133-17.
[2] C. Cheng, X. Xu, Mechanisms of decomposition of metal during femtosecond laser ablation, Phys. Rev. B. 72 (2005) 165415-1–1165415-15.
[3] J. Yang, Y. Zhao, X. Zhu, Theoretical studies of ultrafast ablation of metal targets dominated by phase explosion, Appl. Phys. A 89 (2007) 571–578.
[4] D. Crout, An application of kinetic theory to the problems of evaporation and sublimation of monatomic gases, J. Math. Phys. 15 (1936) 1–54.
[5] Y.V. Martynenko, Y.N. Yavlinskii, Cooling of electron gas of metal at high temperature, Dokl. Akad. Nauk SSSR 270 (1983).
[6] Y.I. Frenkel, Introduction to Theory of Metals, Gos. izd. Fiz-mat. lit., Moskva, 1958.
[7] V.I. Mazhukin, A.V. Mazhukin, O.N. Koroleva, Optical properties of electron fermi-gas of metals at arbitrary temperature and frequency, Laser Phys. 19 (2009) 1179–1186.
[8] K.S. Holian, A new equation of state for aluminum, J. Appl. Phys. 59 (1986) 149–157.
[9] V.E. Fortov, et al. (Eds.), Shock Waves and Extreme States of Matter, Nauka, Moskva, 2000.